scientific reports

Check for updates

OPEN

Development and performance optimization of a taro (*Colocasia esculenta*) peeling machine for enhanced efficiency in small-scale farming

Sandeep Mann[1], Anil Kumar Dixit[2] & Awani Shrivastav[3]✉

Taro (*Colocasia esculenta*) has been a part of traditional cuisine for centuries. Taro contains an alkaloid-containing mucus just beneath the peel that causes itching when it comes into contact with the skin. Manual peeling can easily lead to itchy skin and the long exposure of peeled taro to air causes oxidation, turning the taro yellow and altering its color and flavor. To address the itching problem, a prototype peeling machine was developed. The taro peeling machine mainly comprises a peeling groove, multiple groups of rod-shaped hard brushes (brush rollers), a water spraying mechanism, a sewage outlet, a control system, a frame, and a speed changer device. In this work, a tuber peeling machine was developed and optimized for mother corm peeling. The optimized peeling conditions were found to be the rotating disc speed of 102 rpm, peeling duration of 87 s, and a batch load of 1.7 kg, which yielded a peeling efficiency of 93%, material loss of 8.3%, and peeling effectiveness of 84% were obtained. The peeling machine is designed to peel taro corms of different shapes with higher peeling efficiency and is ideal for small to medium-sized industries. The developed machine reduces the labor intensity, minimizes waste, and enhances the peeling efficiency.

Keywords Taro peeler, Peeling efficiency, Material loss, Optimization, Shaft speed

Taro (*Colocasia esculenta*) is an important tuber crop utilized worldwide in tropical and subtropical regions[1]. Taro holds significant cultural, nutritional, and agricultural value in traditional knowledge across many regions, especially in Asia, the Pacific Islands, and parts of Africa. According to FAOSTAT data[2], Nigeria was the top producer of taro in 2022, with a production of approximately 8.2 million tonnes. Additionally, worldwide production, yield, and the area harvested in the case of taro have increased from 2000 to 2022. Africa accounts for the largest share of global taro production, contributing 82% (Fig. 1). Taro is more abundant and cheaper than other root vegetables like potatoes, carrots, yams, and cassava[3]. Taro is a rich source of vitamins, minerals, carbohydrates, and dietary fiber, making it a great source of nutrition[4]. According to USDA[5] food composition databases, the carbohydrate content in taro is 35 g per 100 g of corm, which is twice that of potatoes. This makes taro a good source of carbohydrates and suitable as a staple food in many countries. It also has 11% protein by dry weight and is rich in vitamin C, minerals, riboflavin, thiamine, and niacin[6]. Taro generally has a short shelf life due to its high moisture content[7]. The most effective way to preserve taro is by obtaining flour and starches. Taro can also be transformed into various value-added products like extruded snacks, bread, noodles, etc.[4].

Regardless of the wide production of taro, and major sources of carbohydrates and other essential nutrients, its use is limited. This is due to low productivity and the presence of anti-nutrients which are harmful and limit the bioavailability of the nutrients[8]. Food made from taro may cause itchiness and inflammation of tissues in some people due to the presence of acrid factors. Acrid factors are the substance that produces a sharp, harsh, or pungent smell or taste. These factors are often associated with certain chemicals or compounds, which when consumed may cause irritation or a burning sensation in the mouth or throat when consumed (Enomfon and Umoh 2004). Acridity in taro is linked to the release of calcium oxalate, which forms very small needle-like crystals called raphides. These crystals can even get into the skin and cause irritation, that ultimately results in

[1]Agricultural Structure and Environment Control Division, ICAR-CIPHET, Ludhiana, Punjab, India. [2]Division of Dairy Economics, Statistics and Management, ICAR-NDRI, Karnal, Haryana, India. [3]Transfer of Technology Division, ICAR-CIPHET, Ludhiana, Punjab, India. ✉email: awani.shrivastav92@gmail.com

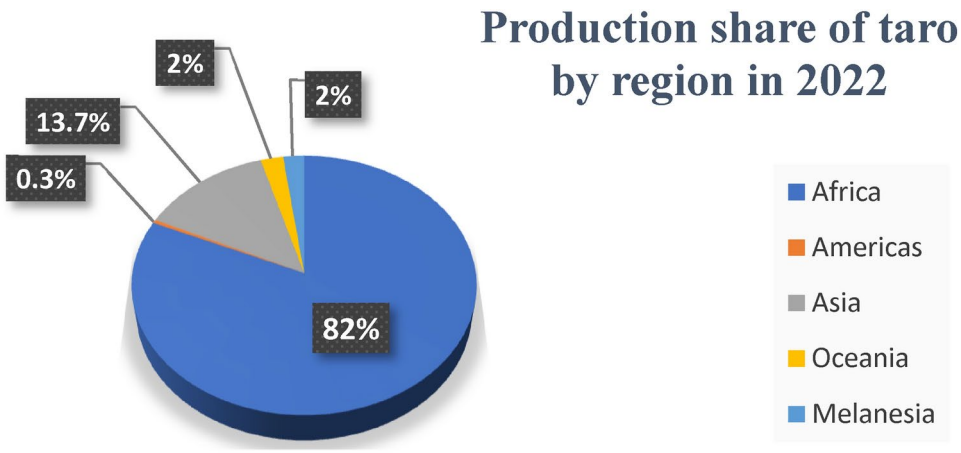

Fig. 1. Production share of taro by region in the year 2022 (Source: FA0STAT 2024).

tissue discomfort. This discomfort prevents animals from consuming raw taro and makes it even more unpleasant for human consumption[9]. According to Chai and Liebman[10], 75% of all kidney stones are comprised primarily of calcium oxalate. Crystal decomposition of calcium oxalate in the kidney and urinary tract are two long-term effects of food containing oxalate[11,12]. To address the issue of acridity factors, peeling, grating, soaking, and fermenting during processing can be applied to reduce their presence[13]. Manual peeling can often lead to skin irritation, while long-time exposure of peeled taro to air can result in oxidation, turning it yellow and changing its color and flavor. Additionally, the manual peeling process takes a long time and requires a lot of labor. This becomes a constraint when production capacity is large and continuous. Therefore, the role of agricultural mechanization is needed to overcome these problems by designing and fabricating a taro peeling machine[14].

Most of the peeling machines available are crop specific like cassava, yam, sweet potatoes, and cocoyam. Balami et al.[15] developed a peeling machine for cocoyam aimed at reducing the drudgery of manual peeling, achieving a maximum peeling efficiency of 68%. Similarly, Ezeanya[16] designed a cocoyam peeling machine and investigated its throughput capacity and peeling efficiency, reporting an improved peeling efficiency of 80%. Ojolo et al.[17] focused on yam peeling and developed a machine incorporating spring-loaded peeling knives and power screw mechanics. Over the years, various peeling machines have been developed and their performance evaluated, with efforts focused on enhancing efficiency[18–21] (Ogunlowo et al. 2016). The problems that arise with peeling machinery available are lower machine efficiency and higher tuber flesh loss. Moreover, the existing commercial peeling machines generally rely on abrasive peeling or knife-based peeling mechanisms, which can lead to excessive material loss, uneven peeling, or inefficiencies in handling the irregular shapes of taro. In this study, a taro peeling machine was designed using brush rollers to achieve efficient peeling. The machine operates on the brush friction principle, a novel technology for peeling taro. Additionally, it is equipped with a water spraying mechanism that helps loosen and soften the peel adhered to the taro corms while simultaneously cleaning the peeled taro. The design was optimized to achieve the highest possible peeling efficiency. Furthermore, the study was conducted to analyze the effect of taro shapes and batch size on the performance matrix of the machine.

Material and methods

Materials

Taro (*Colocasia esculenta*) tubers were procured from local farmers near Ludhiana, Punjab, India. For the study, freshly harvested taro tubers of the *Desi Arbi* (*Punjab Arvi-1*) variety, known for their adaptability and widespread cultivation in Punjab, were selected (Fig. 2). The taro tubers that were too small, contaminated, and damaged were sorted and were not considered for the study. The freshly harvested taro tubes were cleaned to be free from dirt and external contaminants. The taro peeling machine, fabricated with stainless steel grade 304, utilizes a brush friction mechanism, allowing it to efficiently peel multiple taro tubers of different sizes. To ensure optimal peeling, tap water with an adjustable flow rate was used to wet the taro tubers during the peeling process.

Design considerations and criteria

To design a peeling machine for taro, the small entrepreneurs made efforts to make it acceptable and affordable. It was made to be within the buying capacity of local farmers, peel different varieties, shapes, and sizes of taro; made with readily available materials. Stainless steel grade 304 was selected for the fabrication of the taro peeling machine because of its excellent anti-corrosion properties. The machine involves water application and exposure to oxalate-containing taro sap, which can contribute to mild corrosive effects. Stainless steel (grade 304) was chosen as it provides adequate resistance to such conditions while being cost-effective for food processing applications. The taro peeling machine uses the brush friction principle in which multiple rotating brush rollers create friction against the surface of the taro to remove the outer skin. These rollers are arranged in such a way that they maintain uniform contact with taro of various sizes and shapes. The combined action of mechanical brushing and water spray helps to effectively loosen and remove the peel while minimizing damage to the edible portion. The machine is designed so that the capacity of the taro peeling machine is much higher than that of

Fig. 2. (**a**) Samples of taro roots used in the study (**b**) Taro collected after the peeling.

S. No.	Shape	Length (mm)	Diameter (mm)	Mass (g)
1	Cylindrical	148 ± 15	62 ± 8	354 ± 30
2	Oval	216 ± 18	78 ± 12	730 ± 50
3	Irregular	122 ± 12	52 ± 9	245 ± 25

Table 1. Physical properties of taro roots by shape.

the manual peeling method. Therefore, the labor input is considerably reduced and the risk of skin irritation or inflammation from contact with the peel is eliminated. It is important to consider the physical properties of taro, like shape, length, diameter, and mass. Taro is mostly cylindrical or oval, with some irregular shapes. In this design, taro of all shapes and sizes were considered. Around 60 taro samples of different shapes were taken and were categorized according to their three different shapes (cylindrical, oval, and irregular), and mean diameter and mean length were determined by using a vernier caliper and a measuring tape (Table 1).

Based on the data given in Table 1, the overall mean length and diameter of the taro roots of 60 samples were found to be 162 mm and 64 mm, respectively. The mean weight of the 60 taro root samples was found to be 443 g. The design criteria followed consist of determining the volume of the peeling drum, shaft design and its torque, load and twisting moment in the shaft, and power required by the machine.

Determination of volume of peeling drum

The machine was designed to process 3 kg of taro in batches per minute. Therefore, theoretically, the mass of the taro was considered as 3 kg. The volume of each taro root was determined by using the water displacement method, replicating 20 times. The density of each taro root was then calculated based on their masses and volumes, using the method reported by Fadeyibi and Osunde[22]. The average density of 10 samples of each taro root was found to be 1074 kg/m^3. Using the known mass and density, the volume occupied by the taro roots can be computed using the equation given below,

$$\rho = \frac{m}{v} \tag{1}$$

where, m, ρ, and v are the mass, density, and volume of the taro roots, respectively. The volume of the peeling drum was kept slightly higher than the processing capacity of the taro. After finding out the volume of the peeling drum (V), the length, width, and height of the peeling drum were found out.

Shaft design and torque calculation

The shaft design in a peeling process involves the determination of shaft diameter, selecting an appropriate material for it, and ensuring the factor of safety. Stainless steel (Grade 304) was selected because of its excellent anti-corrosion properties. The diameter of the shaft was calculated from the torque required without exceeding the allowable shear stress of the material. Equation 2 was used in order to obtain the diameter (d) of the shaft.

$$d = \left(\frac{16T}{\pi\tau}\right)^{1/3} \tag{2}$$

where T is Torque (N-m), τ is the allowable shear stress which was obtained from the yield strength of the material. A factor of safety value of 1.5–2 was considered to avoid failure at unexpected loads.

From the design point of view, it was considered that the peeling force is applied evenly along the surface of the rollers. The peeling force (F) is determined based on the interaction between the taro skin and the rollers, considering the required frictional force to achieve effective peeling. The torque required was calculated as a product of the peeling force on each roller (F) and the radius of the shaft (r) as given in Eq. 3.

$$T = F \times r \tag{3}$$

The total torque required was calculated as the sum of the total torque required (T_{total}) for each roller (Eq. 4).

$$T_{total} = \sum T_i \tag{4}$$

where T_i is the torque required in each roller (N-m).

Load and twisting moment calculation

While carrying out the peeling operation, the shaft experiences different loads i.e., torsional load, bending load, and axial loads. The primary load is the torsional or twisted load which occurs due to the torque transmitted by the shaft to the rollers. This was previously calculated using Eq. 3. The bending load or bending moment acting on the shaft depends upon the weight of the rollers, taro roots, or any other component mounted on the shaft. The bending moment (M), torque (T), and diameter of the shaft (d) are related to maximum torsional stress (τ_{max}) (Khurrmi and Gupta 2008), which can be calculated as

$$\tau_{max} = {}^{1}/_{2}\sqrt{(\delta b)^2 + 4\tau^2} \tag{5}$$

δb is the bending stress (tensile or compressive) induced stress due to moment. For the shaft material SS-304, δb was taken as 150 MPa. To determine the bending moment of inertia (M), Eq. 6 can be used.

$$\tau_{max} = \frac{16}{\pi d^3}\left(\sqrt{M^2 + T^2}\right) \tag{6}$$

It is important to consider the combined stress when both torsion and bending loads are involved. Von Mises criteria can be used in order to analyze the combined stress. Von Mises criteria are helpful in determining the yielding of materials under any load condition from the combination of stresses. This is crucial in determining the safety of a structure that is subjected to different loads.

$$\sigma_{combine} = \sqrt{\left(\frac{\sigma_{bending}}{2}\right)^2 + 3\left(\frac{\tau_{torsion}}{2}\right)^2} \tag{7}$$

where, $\sigma_{combine}$, $\sigma_{bending}$, and $\tau_{torsion}$ are the combined stress, bending stress, and shear stress due to torsion.

Power requirement for the machine

The power requirement for the taro peeling machine is an important design consideration to ensure efficient operation, especially for small entrepreneurs and local farmers. The machine is designed to process 3 kg of taro per minute and the power needed to achieve this capacity was determined by analyzing the frictional forces, torque, and mechanical efficiency of the system. The mechanical power (*P*) required was then calculated using the formula

$$P = T \cdot \omega \tag{8}$$

where P is power (Watt), T is the total torque (N-m) (calculated in Eq. 4), and ω is the rotational speed (rad/s).

Machine description

The taro peeling machine, designed to handle 3 kg of taro tubers per minute in batch processing, was developed and fabricated at the workshop of ICAR-CIPHET, Ludhiana, Punjab, India. Figure 3a shows the CAD model representation of the developed machine and an image of the developed prototype, with all components labeled. The Taro peeling machine consists of five rollers with 45 mm diameter and 102 mm long each. The rollers are mounted over a shaft of 25 mm diameter. The main components of the unit were (1) a peeling Chamber, (2) a power transmission system (3) a water spray system. The taro peeling machine operates using the brush friction principle, ensuring efficient skin removal while minimizing damage to the edible portion. Raw taro tubers are loaded into the peeling chamber, where five concavely arranged brush rollers rotate clockwise, creating friction against the surface of the anticlockwise rotating tubers (Fig. 3b). This friction effectively scrubs off the outer skin. A water spray system continuously washes away loosened peels and prevents overheating. The machine's Variable Frequency Drive (VFD) allows speed adjustments to accommodate different tuber sizes and skin textures. Once

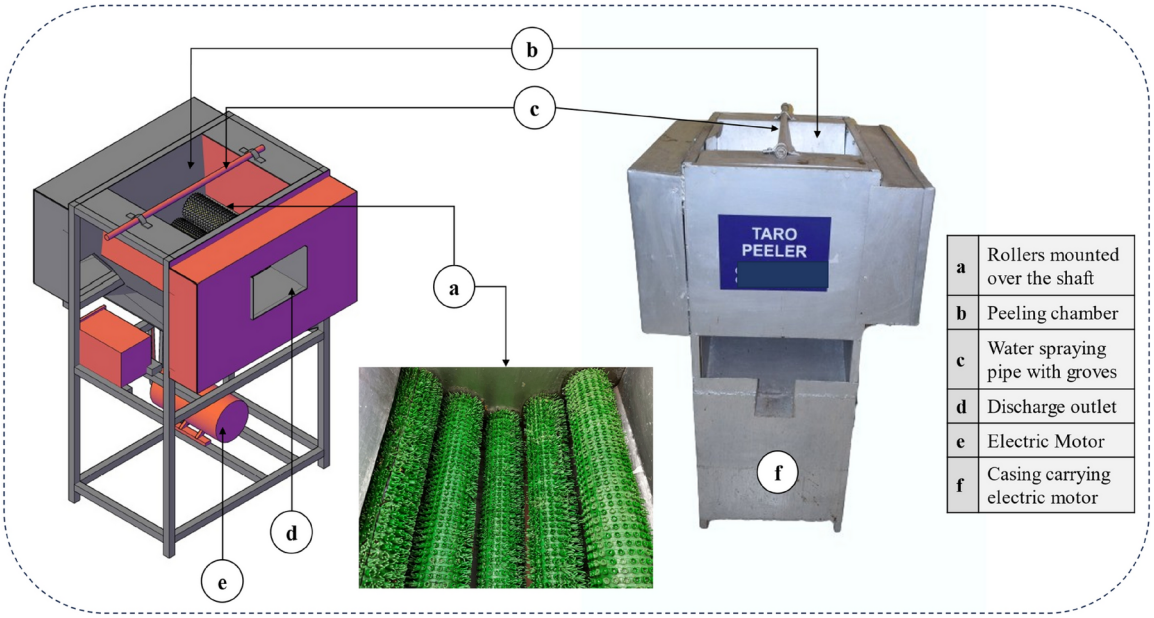

(a)

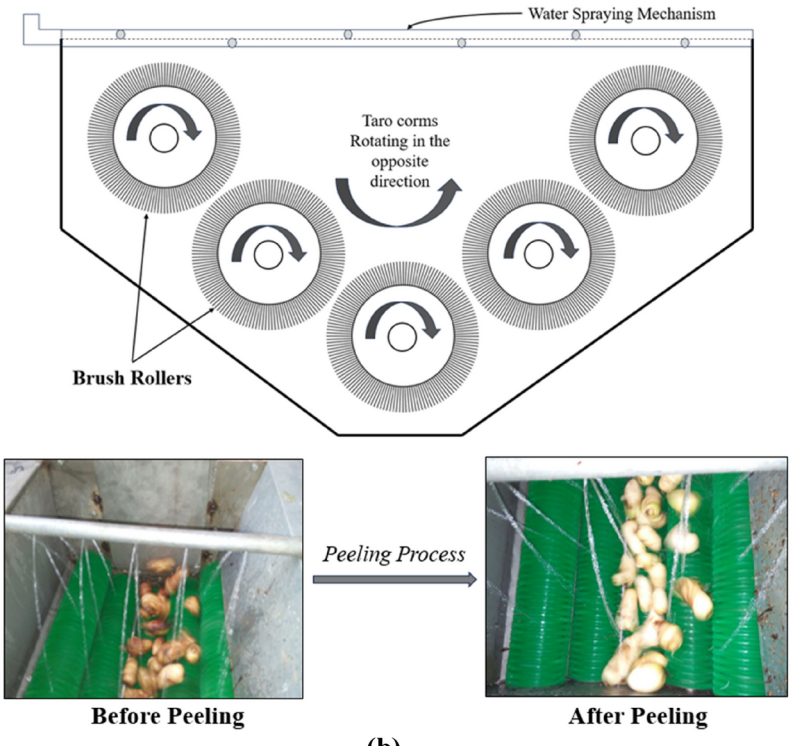

(b)

Fig. 3. (**a**) CAD model and developed prototype of the taro peeling machine. (**b**) Schematic showing the peeling mechanism and the tubers before and after peeling.

peeling is complete, the peeled taro is discharged, and waste peels are flushed out, ensuring a clean and efficient operation. The hollow pipe frame of the machine was fabricated in a rectangular shape to provide strength and firmness to the machine. The prototype is 470 mm wide, 750 mm long, 960 mm high, and fabricated with mild steel square pipe 25 mm × 25 mm × 1.25 mm. The body was covered using a stainless steel sheet to avoid rusting. Five brush rollers (45 mm diameter) were also installed in a concave shape to enhance the effect of friction. A provision was made to spray water while running the machine. It receives torque from a 1 HP (0.746 kW) electric

motor with a speed of 1500 rpm. The drive system consists of a belt and pulley arrangement with maximum machine speeds of 750 rpm, with speed variations controlled by a variable frequency drive (VFD). The design of various components of the integrated unit was mainly based on the functional and structural strength and was checked mathematically. The specification of the machine is given in tabular form in Table 2.

Experimental setup

Peeling experiments were conducted to study the effect of operating parameters on achieving efficient peeling of taro tubers with minimal material loss. The optimal peeling conditions were defined based on measurable parameters, including peeling efficiency (%), material loss (%), and peeling effectiveness (%). The experiments tested different roller speeds of 60, 100, and 140 rpm, and varying peeling durations of 60, 90, and 120 s. These levels were determined through preliminary studies. It was observed that operating the peeling machine at full capacity is not recommended as it reduces its effectiveness. Therefore, the effectiveness of different batch loads was also considered. Three levels of batch load 1 kg, 2 kg, and 3 kg—were tested to assess the effectiveness of the peeling. The peeling performance was evaluated using three metrics: peeling efficiency (η_p), material loss (ML), and peeling effectiveness (PE). The response variables like peeling efficiency, material loss, and peeling effectiveness were considered for the study because they are critical indicators of the machine's performance, efficiency, and overall effectiveness in peeling taro (Nagar et al. 2022). Before conducting the experiments, the theoretical percentages of peel and flesh were determined by manually removing the peelings from raw taro using a knife.

Different peeling quality factors were calculated using Eq. (9) to (13) [21].

$$\text{Actual Peel Content, } P_{th}\,(\%) = \frac{M_{thp}}{M_t} \times 100 \tag{9}$$

$$\text{Actual Flesh Content, } F_{th}\,(\%) = \frac{M_t - M_{thp}}{M_t} \times 100 \tag{10}$$

$$\text{Peeling Efficiency, } \eta_p\,(\%) = \frac{(M_{sp} \times P_{th}) - M_{rp}}{(M_{sp} \times P_{th})} \times 100 \tag{11}$$

$$\text{Material loss, ML } (\%) = \frac{(M_{sp} \times F_{th}) - (M_{psp} - M_{rp})}{(M_{sp} \times F_{th})} \times 100 \tag{12}$$

$$\text{Peeling Effectiveness, PE}\,(\%) = (1-\text{ML}) \times \eta_\text{p} \times 100 \tag{13}$$

where P_{th} = theoretical peel content; M_{thp} = weight of peel obtained by manual peeling (theoretical peel weight); M_t = weight of corms taken for manual peeling; F_{th} = theoretical flesh content; η_p = peeling efficiency; ML = material loss; M_{sp} = weight of taro corms fed into the peeler; M_{rp} = weight of peel retained on the peeled tuber collected at the outlet of the peeler; and M_{psp} = weight of peeled taro corm obtained at the outlet of the peeler.

In addition to this, the impact of taro shapes (cylindrical, oval, irregular) and batch load (1 kg, 2 kg, 3 kg) on peeling efficiency, material loss, and peeling effectiveness was studied. For this taro corms of different shapes were sorted manually based on visual appearance. Cylindrical corms were long and evenly shaped with a consistent width, oval corms were slightly rounded with some variation in size, and irregular corms had uneven and unpredictable shapes.

Statistical analysis

Response Surface Methodology (RSM) is an effective technique for fitting a quadratic surface and it helps in optimizing process parameters with a minimal number of experiments. It also helps in analyzing the interaction among different parameters[23]. It is also one of the economical methods for carrying out statistical data analysis[24]. In this study, a Central Composite Rotatable Design (CCRD) was applied and three parameters with different levels were taken into consideration, to minimize the number of experiments performed and optimize the

Specification	Details
Design capacity	≈ 200 kg/h
Shaft diameter	25 mm
Number of rollers	5
Roller diameter	45 mm
Roller length	102 mm
Prototype dimensions	470 mm (W) × 750 mm (L) × 960 mm (H)
Frame dimensions	25 mm × 25 mm × 1.25 mm
Body cover material	Stainless steel sheet
Body cover thickness	95 mm
Motor power	1 HP (0.746 kW)

Table 2. General specifications of taro peeling machine.

Independent variable	Coded variable levels				
	− α − 1.68	Low − 1	Medium 0	High 1	+ α + 1.68
Roller speed (A)	33.33 rpm	60 rpm	100 rpm	140 rpm	166.67 rpm
Time of operation (B)	40 s	60 s	90 s	120 s	140 s
Batch load (C)	0.33 kg	1 kg	2 kg	3 kg	3.67 kg

Table 3. Levels of various parameters used in CCRD for peeling taro mother corms.

Run No.	Roller speed (rpm)	Peeling time (s)	Batch load (kg)	Peeling efficiency (%)	Material loss (%)	Peeling effectiveness (%)
1	60	120	1	73.12	12.84	63.45
2	100	90	2	91.87	9.23	83.22
3	167.27	90	2	77.95	33.57	52.12
4	32.73	90	2	58.21	13.62	50.47
5	100	39.55	2	76.02	10.42	68.13
6	60	60	1	65.34	10.12	58.67
7	140	60	3	77.56	20.34	63.12
8	100	90	3.68	86.22	18.47	70.04
9	60	60	3	61.89	14.67	54.02
10	140	60	1	82.76	16.78	70.41
11	60	120	3	66.78	20.95	53.55
12	100	90	2	90.78	12.04	79.12
13	100	90	2	96.12	9.41	80.67
14	100	140.45	2	80.02	17.89	66.02
15	100	90	2	90.23	5.41	86.92
16	100	90	2	91.02	8.89	82.45
17	100	90	0.32	88.76	14.92	75.23
18	140	120	1	88.95	27.56	65.12
19	100	90	2	94.02	9.78	83.55
20	140	120	3	81.76	30.42	58.02

Table 4. CCD Experimental runs and corresponding responses for taro peeling machine.

peeling conditions. The regression analysis was conducted using Design Expert software (Stat-Ease, Statistics Made Easy, Minneapolis, MN, USA), and the results were validated through analysis of variance (ANOVA) and the F-test.

Results and discussion

Optimizing operational parameters for peeling taro mother corms

The theoretical peel content and flesh content of taro mother corms were found to be 15.74 ± 0.65% and 84.26 ± 0.74%, respectively. The peeling efficiency (η_p) by manual peeling was 97.46 ± 0.52%. Material loss (ML) and peeling effectiveness (PE) in the case of manual taro peeling were obtained to be 0.055 ± 0.11%, and 92 ± 0.33%, respectively. The manual peeling method took about 30 to 35 min per kg of taro peeling.

The main variables that were considered for the study were roller speed (rpm), operating time (s), and batch load (kg) as given in Table 3. A quadratic model was fitted and ANOVA was performed in order to identify the significant effects of independent parameters on peeling process response parameters. Table 4 indicates central composite design (CCD) results and the responses obtained in the taro peeling machine. In the subsequent section, the effect of independent parameters on peeling efficiency, material loss, and peeling effectiveness are presented and discussed.

Impact of process parameters on peeling efficiency (η_p) of taro corm

The peeling efficiency was varied from 62.1 to 96.7%. The highest peeling efficiency i.e., 96.75% was obtained at roller speed of 100 rpm, peeling time of 90 s, and batch load condition of 2 kg. This optimal combination likely maximizes the friction and mechanical action on the taro corms, ensuring thorough peeling. On the other hand, the lowest peeling efficiency i.e., 62.11% was recorded at a roller speed of 60 rpm, peeling time of 60 s, and batch load condition of 3 kg. The reduced speed and time likely provided insufficient friction and contact for effective peeling, while the larger batch load may have caused overcrowding, further diminishing the efficiency of the process.

Table 5 gives the (ANOVA) results of peeling efficiency for fitting the quadratic model to experimental data. The regression model for peeling efficiency was found to be statistically significant at a 95% confidence

Source	Peeling efficiency (%)		Material Loss (%)		Peeling effectiveness (%)	
	P value	Regression coefficient	*P* value	Regression coefficient	*P* value	Regression coefficient
Model	< 0.0001*	92.75	< 0.0001*	8.59	< 0.0001*	83.58
A—Roller speed	< 0.0001*	7.28	< 0.0001*	4.72	0.1609	1.63
B—Peeling time	0.0283**	2.27	0.0007*	3.32	0.5215	− 0.7140
C—Batch load	0.0572***	− 1.89	0.0209**	1.88	0.0203**	− 2.96
AB	0.8093	− 0.2863	0.1110	1.57	0.2002	− 1.93
AC	0.6361	− 0.5638	0.4283	− 0.7425	0.9855	0.0262
BC	0.6480	− 0.5438	0.6796	0.3825	0.6516	− 0.6537
A^2	< 0.0001*	− 8.37	< 0.0001*	4.74	< 0.0001*	− 11.01
B^2	< 0.0001*	− 5.90	0.0114**	2.07	< 0.0001*	− 6.60
C^2	0.0197**	− 2.39	0.0006*	3.28	0.0014*	− 4.58

Table 5. ANOVA for the effect of process parameters on peeling efficiency, material loss, and peeling effectiveness of taro corm. ***—Significant at 0.1 level ($P \leq 0.1$), **—Significant at 0.05 level ($P \leq 0.05$), *—Significant at 0.001 level ($P \leq 0.001$).

level. The lack of fit values was found to be non-significant with a confidence level of 92.5% (adjusted R^2). To assess the adequacy of the regression model, the values of R^2, adjusted R^2, and the coefficient of variation (CV) were determined. The high level of variability in the response, with R^2 exceeding 95%, indicates that the model reliably explains the peeling efficiency. An empirical model was developed, expressed in terms of coded factors, to express the relationship between the independent parameters and peeling efficiency (Eq. 14).

$$\text{Peeling Efficiency}\,(\%) = +92.75 + 7.28\text{A} + 2.27\text{B} - 1.89\text{C} - 8.37\text{A}^2 - 5.90\text{B}^2 - 2.39\text{C}^2 \left(\text{R}^2 = 0.96\right) \quad (14)$$

Table 5 and the coded regression equation for peeling efficiency (Eq. 14) demonstrate that roller speed, peeling time, and batch load significantly affect peeling efficiency at the linear level with $P \leq 0.001$, $P \leq 0.05$, and $P \leq 0.005$, respectively. Equation 14 indicates the peeling efficiency is highly affected by the roller speed, followed by peeling time (7.28 and 2.27, respectively), while the negative coefficient for batch load condition (− 1.89) indicates that higher batch loads reduce efficiency. The quadratic terms (A^2, B^2, C^2) also play significant roles, with negative coefficients suggesting diminishing returns or negative effects at higher levels.

Figure 4 depicts the 3D response surface plots of the variation of peeling efficiency with roller speed, peeling time, and batch load condition. The primary influencing parameters that affect the peeling efficiency were found to be roller speed and peeling time. From the results, it can be observed that the peeling efficiency increased up to an optimum level and then started decreasing in the case of roller speed and peeling duration. This behavior suggests that while higher roller speeds and longer peeling times initially enhance the efficiency by increasing friction and contact, beyond the optimum levels, these factors may lead to over-peeling or mechanical damage, thereby reducing overall efficiency. Olukunle and Akinnuli[25] and Daniyan et al.[26] also observed similar trends in the research carried out in the case of cassava tubers. The peeling efficiency also increased by increasing the batch load up to a certain peeling duration after which it starts decreasing due to over peeling of taro corm.

Impact of process parameters on material loss of taro corm

Material loss (ML) is an important parameter to measure because it affects the yield and efficiency of the peeling process. The ML was found to vary between 3.5% and 31.04%. The lowest ML value was observed at the roller speed of 100 rpm, peeling time of 90 s, and batch load condition of 2 kg. On the other hand, the highest ML value was obtained at the roller speed of 140 rpm, peeling time of 120 s, and batch load condition of 3 kg. The higher roller speed and longer peeling time increase the likelihood of over-peeling, while the larger batch load may contribute to uneven peeling, both of which result in greater material loss.

Table 5 presents the ANOVA results for ML based on fitting the quadratic model to the experimental data. The regression model for ML was found to be statistically significant with a 95% confidence level. The lack of fit values was non-significant, with a confidence level of 92.5% (adjusted R^2). To assess the adequacy of the regression model, the values of R^2, adjusted R^2, and the coefficient of variation (CV) were calculated. The high variability in the response, indicated by an R^2 value exceeding 95%, demonstrates that the model reliably explains the ML. An empirical model, expressed in terms of coded factors, was developed to describe the relationship between the independent parameters and ML (Eq. 15).

$$\text{Material Loss}\,(\%) = +8.59 + 4.72\text{A} + 3.32\text{B} + 1.88\text{C} + 4.74\text{A}^2 + 2.07\text{B}^2 + 3.28\text{C}^2 \left(\text{R}^2 = 0.94\right) \quad (15)$$

Table 5 and the coded regression equation for ML (Eq. 15) demonstrate that roller speed, peeling time, and batch load significantly affect ML at the linear level with $P \leq 0.001$, $P \leq 0.05$, and $P \leq 0.05$, respectively. Equation 15 explains how much material is lost during the taro peeling process based on roller speed (A), peeling time (B), and batch load (C). The starting value of 8.59% shows the material loss when all other factors are zero. The terms 4.72A, 3.32B, and 1.88C mean that increasing roller speed, peeling time, and batch load will each increase the

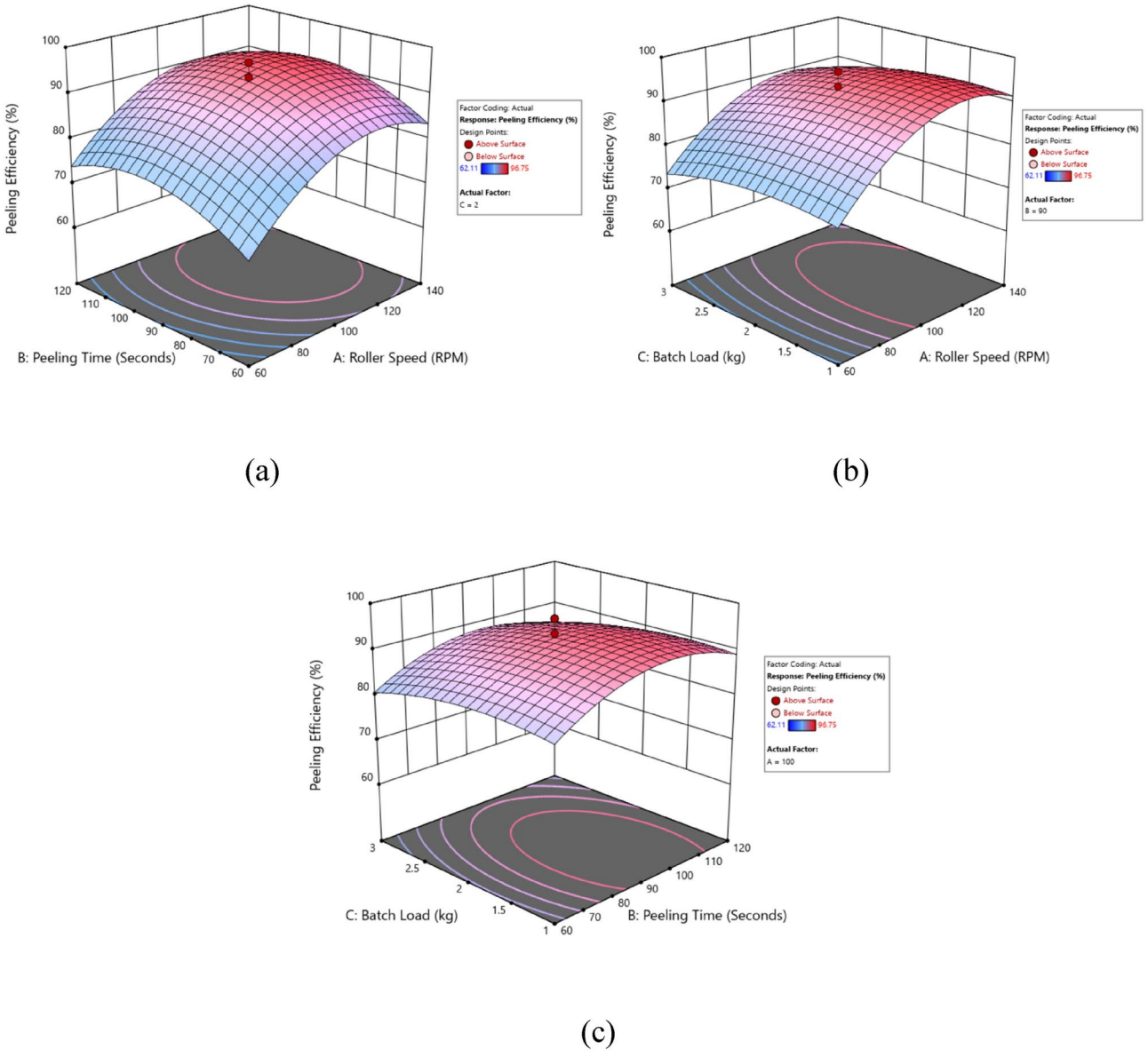

Fig. 4. 3-D response surface plots of the variation of peeling efficiency under different independent variable conditions.

material loss. The terms $4.74A^2$, $2.07B^2$, and $3.28C^2$ show that very high values of these factors lead to a much larger increase in material loss.

Figure 5 depicts the 3D response surface plots of the variation of ML with roller speed, peeling time, and batch load condition. The ML starts to decrease up to an optimum level and then starts increasing. This phenomenon can be attributed to the dynamics of the peeling process. At higher speeds and longer peeling durations, the tubers make less frequent contact with the roller's surfaces. As a result, the initial reduction in material loss is due to the efficient removal of the peel without significant loss of the flesh. However, beyond the optimal point, the efficiency drops, causing an increase in material loss. This increase is due to the prolonged exposure to the roller surfaces, which leads to the removal of flesh portions along with the peel. Fadeyibi and Faith Ajao[18] also reported in their research findings the mechanical damage of tuber at higher peeling speeds, which results in a reduction in the mass of the peeled tubers. The ML was also found to decrease at an optimum batch load condition, after which it started increasing. At optimal load, tubers interact efficiently with roller surfaces, minimizing loss. Beyond this load, overcrowding reduces effective contact, increasing material loss as both skin and flesh are removed. Therefore, maintaining the optimal batch load is essential for efficient peeling with minimal material loss. Similar findings were reported in the case of potato peeling by Singh and Shukla[27].

Impact of process parameters on peeling effectiveness of taro corm

Peeling effectiveness (PE) measures how well the peeling process removes the skin while minimizing the loss of edible flesh. The PE was found to vary between 52.77 and 89.05% for different combinations of process parameter

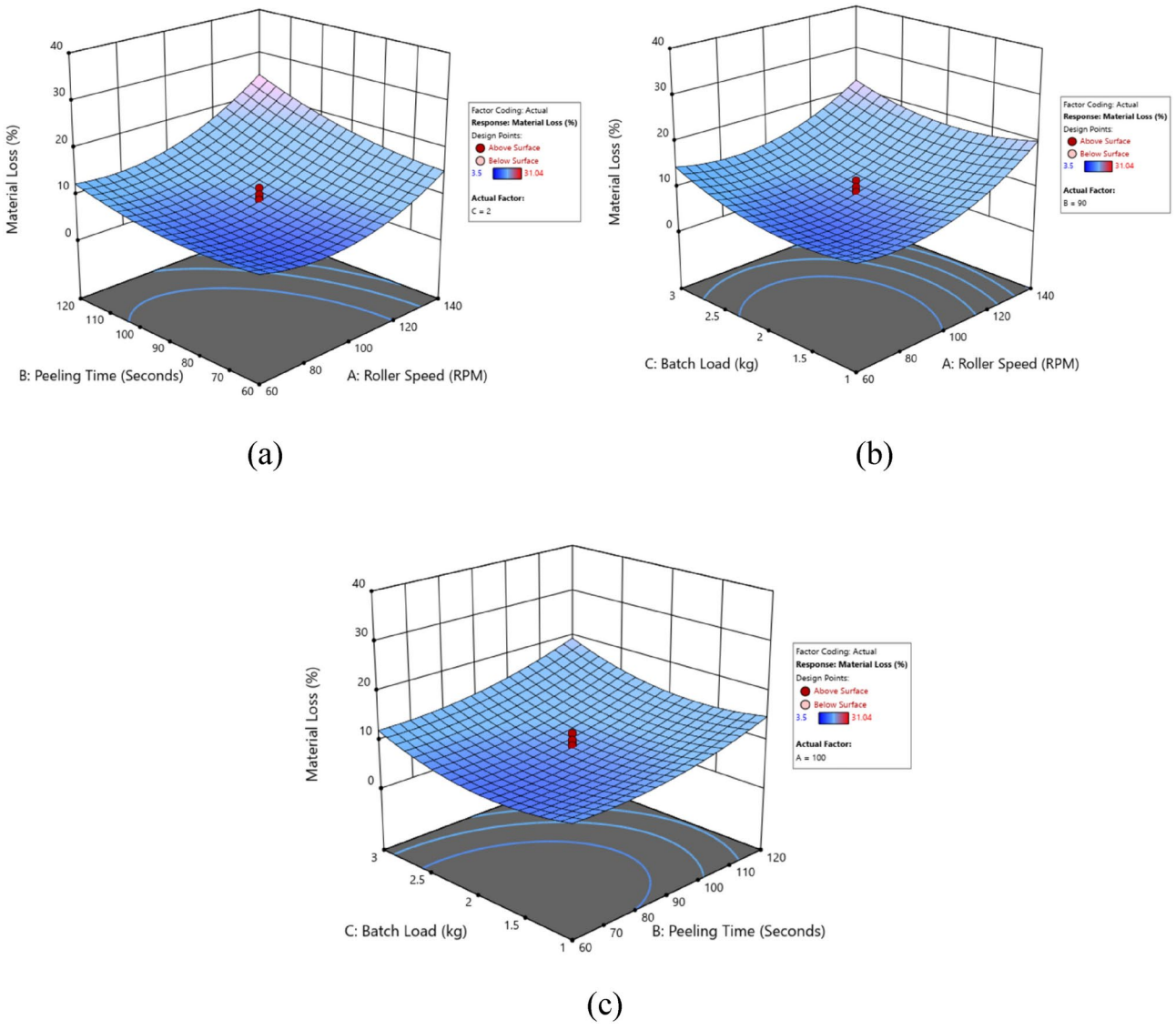

Fig. 5. 3-D response surface plots of the variation of ML under different independent variable conditions.

conditions. The lowest value of peeling effectiveness i.e., 52.77% was observed at roller speed of 60 rpm, peeling time of 120 s, and batch load condition of 3 kg. At lower roller speeds and longer peeling times with a higher batch load, the tubers may not have enough effective contact with the roller surfaces. The extended peeling time can cause excessive wear on the flesh, leading to higher material loss and lower peeling effectiveness. The highest value of peeling effectiveness i.e., 89.05% was observed at roller speed of 100 rpm, peeling time of 90 s, and batch load condition of 2 kg. At an optimal roller speed and moderate peeling time with a smaller batch load, the tubers achieve better contact with the rollar surfaces, resulting in effective skin removal with minimal loss of edible flesh. The balance of these parameters optimizes the peeling process, leading to higher peeling effectiveness.

Table 5 shows the ANOVA results for peeling effectiveness (PE) using a quadratic model fit to the experimental data. The regression model for PE was statistically significant at a 95% confidence level. The lack of fit was non-significant, with a confidence level of 90.7% (adjusted R^2). To evaluate the regression model's adequacy, the R^2, adjusted R^2, and coefficient of variation (CV) were calculated. The high R^2 value, exceeding 95%, indicates that the model reliably explains the variation in PE. An empirical model, described by coded factors, was developed to express the relationship between the independent parameters and PE (Eq. 16).

$$\text{Peeling Effectiveness}\,(\%) = +83.58 + 1.63\text{A} - 0.71\text{B} - 2.96\text{C} - 11\text{A}^2 - 6.6\text{B}^2 - 4.58\text{C}^2 \qquad (16)$$

Table 5 and the coded regression equation for PE (Eq. 16) demonstrate that roller speed, peeling time, and batch load significantly affect PE at the linear level with $P \leq 0.001$, $P \leq 0.05$, and $P \leq 0.05$, respectively. The positive linear coefficient of roller speed (1.63) indicates an initial enhancement in PE with increased speed, while negative coefficients for peeling time (−0.71) and batch load (−2.96) suggest a reduction in PE as these parameters

rise. This model highlights the need to find the best settings for roller speed, peeling time, and batch load to maximize peeling effectiveness. It shows how these factors interact in a complex way to ensure efficient peeling with minimal loss of edible flesh.

Figure 6 depicts the 3D response surface plots of the variation of PE with roller speed, peeling time, and batch load condition. The trend of PE was found similar to peeling efficiency at different process parameter conditions. This could be due to the surface features of the tuber and uneven peeling when there are too many tubers being peeled at once. Additionally, differences in the sizes of the tubers in the batch might have affected how well they were peeled. Similar findings were also reported by Nagar et al.[28], while observing the effect of independent parameters on peeling effectiveness of mother corm.

Numerical and graphical optimization of independent parameters

To determine the best peeling conditions for taro, the process parameters (roller speed, peeling time, and batch load) were optimized. This optimization was carried out using both numerical and graphical methods with Design Expert software. The goal was to achieve maximum peeling efficiency while minimizing material loss. The optimization was based on the desirability function technique, which scales the response parameters from 0 (undesirable) to 1 (most desirable). The target for each parameter was set to achieve the best peeling efficiency with minimal material loss. Specifically, peeling efficiency and peeling effectiveness were aimed at their maximum values, while material loss was minimized. The weights of these parameters were adjusted to balance their contributions.

The optimal solution was identified by maximizing the desirability score. For this case, the optimal values were found to be a roller speed of 101.91 rpm, a peeling time of 87.43 s, and a batch load of 1.68 kg. For practical purposes, these values can be rounded to a roller speed of 102 rpm, a peeling time of 87 s, and a batch load of

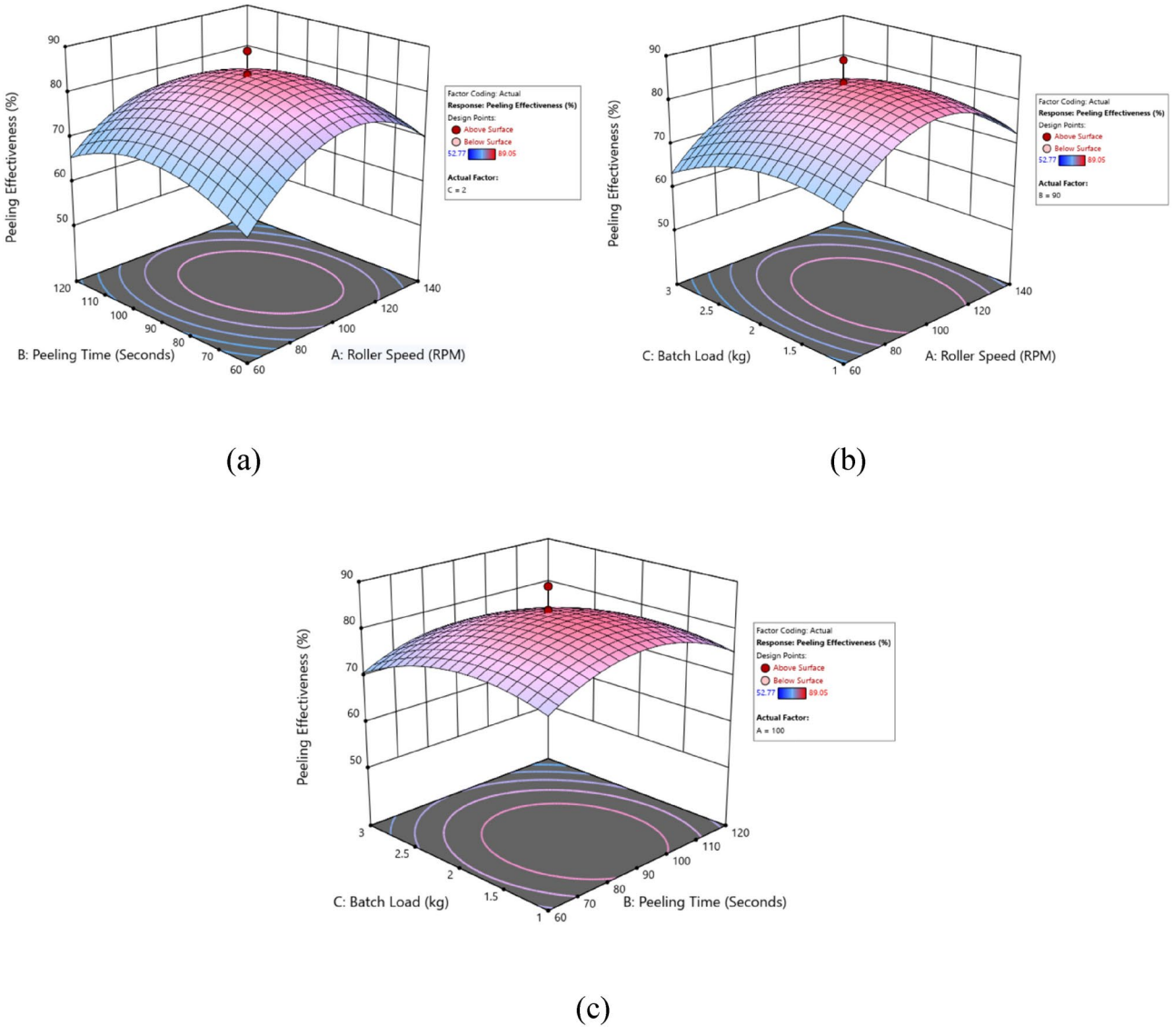

Fig. 6. 3-D response surface plots of the variation of PE under different independent variable conditions.

1.7 kg. Figure 7 shows the interaction plot of the different responses. The optimal conditions—roller speed of 102 rpm, peeling time of 87 s, and batch load of 1.7 kg—achieved the highest peeling efficiency (93%), peeling effectiveness (84%), and lowest material loss (8.3%). Although the design capacity of the peeling machine is 3 kg per batch, experimental results indicated that operating at 1.7 kg yields the highest peeling efficiency while minimizing material loss. This is due the reason that the optimized batch load prevents overcrowding and ensures even friction between the taro corms and the brush rollers. For small-scale taro farmers, this machine is much faster than peeling by hand. Manual peeling takes about 30–35 min for 1 kg of taro, but this machine can peel 1.7 kg in just 87 s. This saves a lot of time and effort, making it very useful for farmers and small processing units.

Performance of the taro peeling machine under varying conditions

Figure 8 compares the performance of the taro peeling machine under varying conditions of taro shape, and batch size. Peeling efficiency, representing the percentage of peel removed, is highest for cylindrical shapes (94.5%), followed by oval (93.1%) and irregular shapes (92.0%), with smaller batch sizes (1 kg) giving better results due

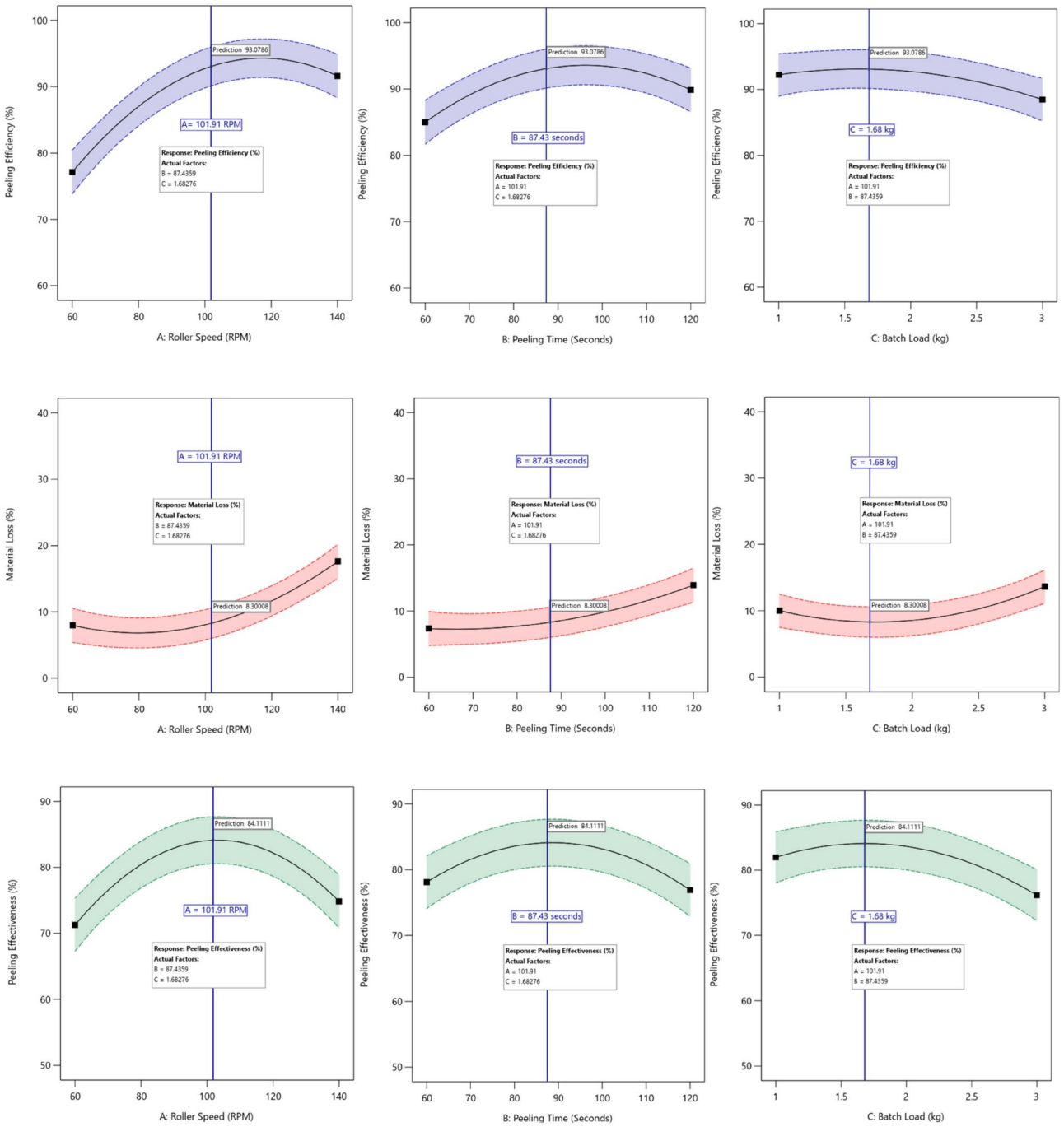

Fig. 7. Interaction plot of peeling process parameters for taro corm.

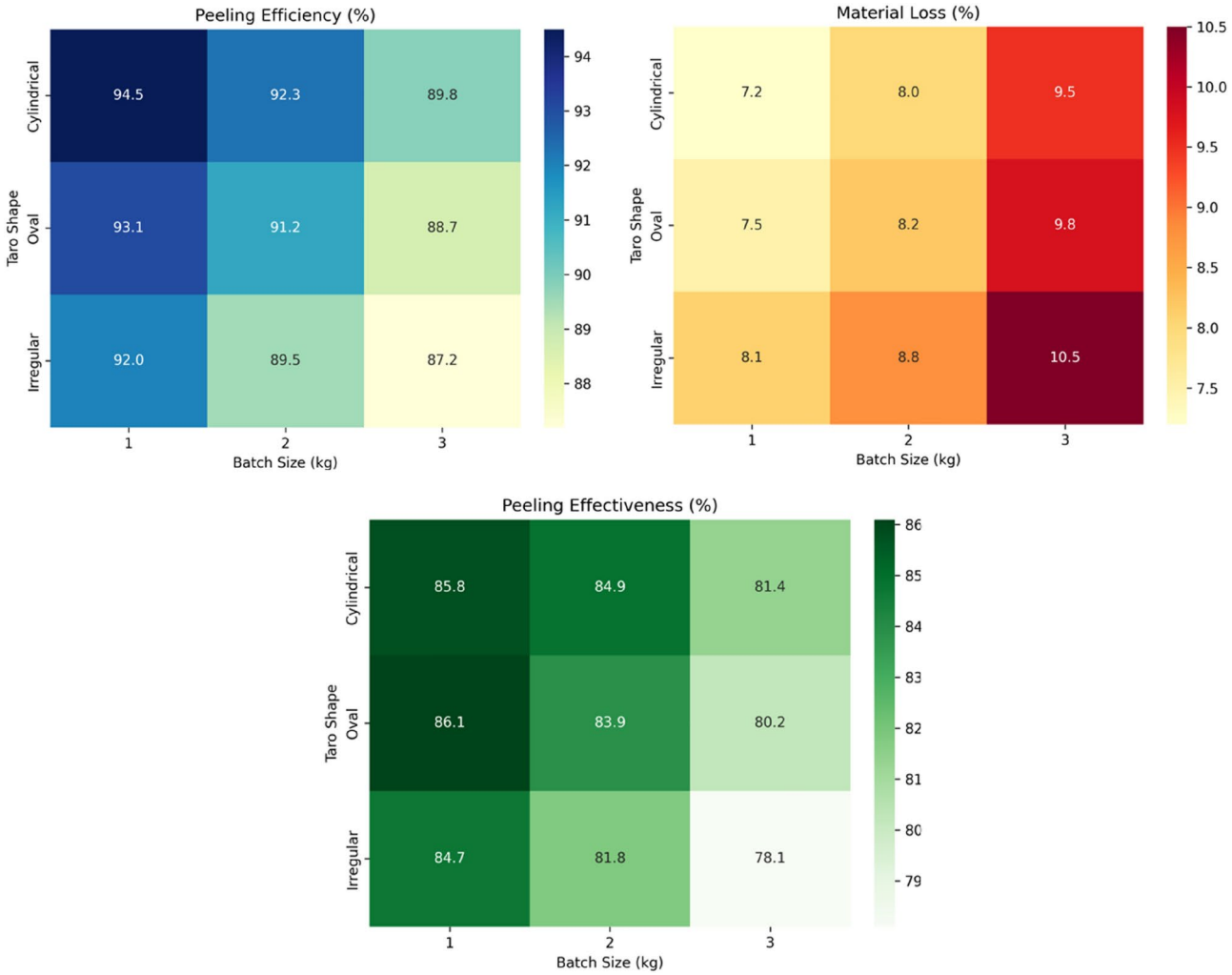

Fig. 8. Performance of the taro peeling machine for different taro corm shapes.

to reduced overcrowding and improved contact with brush rollers. Material loss is lowest for cylindrical shapes (7.2% at 1 kg), followed by oval (7.5%) and irregular shapes (8.1%), and increases with larger batches (up to 10.5% for irregular taro at 3 kg) due to excessive contact with roller surfaces. Peeling effectiveness is highest for cylindrical shapes (85.8% at 1 kg) and lowest for irregular shapes (78.1% at 3 kg), with medium batch sizes (2 kg) striking the optimal balance between efficiency and minimal loss. Overall, cylindrical shapes and smaller to medium batch sizes (1–2 kg) consistently deliver the best performance, emphasizing the importance of uniformity in shape and controlled batch sizes for optimal machine operation. These findings underscore the need for improved adaptability to irregular shapes and guide further design optimizations for broader usability.

The bar graph (Fig. 9) shows the comparative analysis of peeling efficiency, material loss, and peeling effectiveness with different taro shapes highlighting how shape influences the performance of the peeling machine. Cylindrical shapes achieve the highest peeling efficiency (94.5%) due to their smooth and uniform surfaces, which enhance friction with the machine's brush rollers. Material loss is lowest for cylindrical shapes (7.2%), slightly higher for oval shapes (7.5%), and highest for irregular shapes (8.1%) due to uneven surfaces that cause over-peeling. Fadeyibi and Faith Ajao[18], in their study, also discussed that the more irregular the shape of root crops, the greater the material loss. Peeling effectiveness, which combines efficiency and material loss, is highest for oval shapes (86.1%). Overall, cylindrical shapes are ideal for maximizing peeling efficiency and minimizing material loss, while oval shapes strike a balance, which leads to the highest overall effectiveness. The results indicate that the machine works well with uniform shapes, and adding features like adjustable roller surfaces could make it better at handling irregular taro shapes.

Conclusion

A Taro peeling machine, adaptable for various root crops, was successfully designed, and developed, and its performance was thoroughly evaluated. Since taro contains an alkaloid-containing mucus beneath its peel that can cause skin irritation and itching, a specialized prototype was created to resolve this issue, effectively eliminating the discomfort associated with manual peeling. The peeling machine consists of five brush rollers for

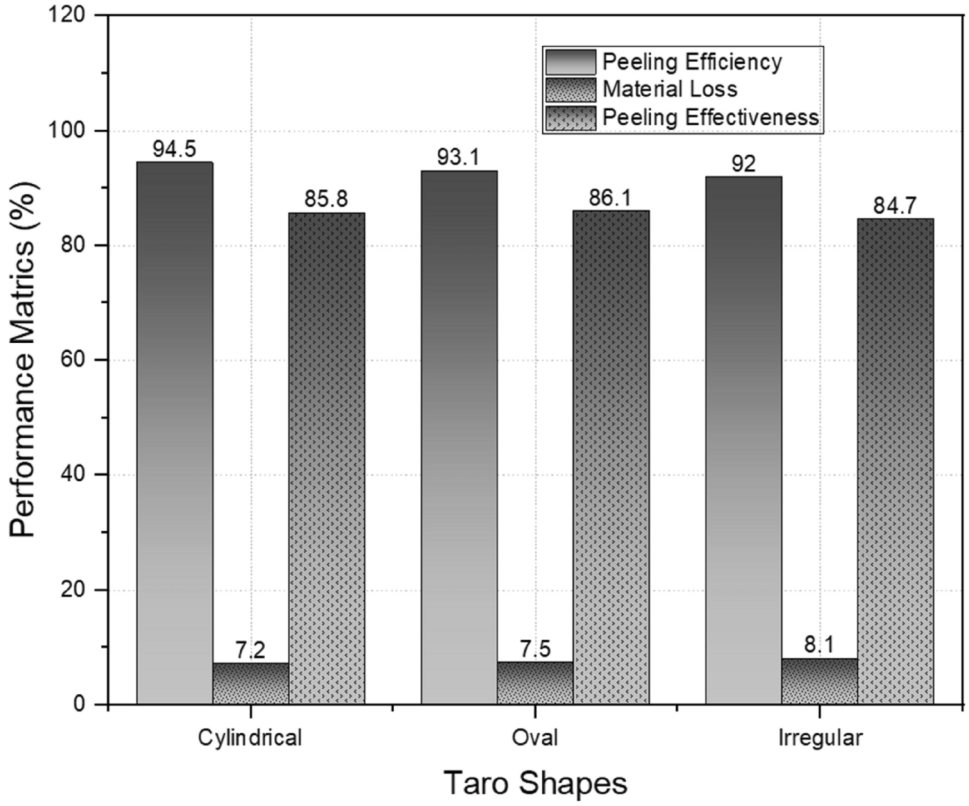

Fig. 9. Performance metrics comparison of different taro shapes.

peeling the taro corms. The water spraying mechanism provided in the machine performs multiple operations like washing the taro corms and loosening the peel adhered to the taro corms which helps in peeling efficiently. This study investigated the optimal peeling parameters for mother corms. Response Surface Methodology (RSM) combined with Central Composite Rotatable Design (CCRD) was employed to achieve maximum peeling efficiency and effectiveness while minimizing material loss. The optimized conditions were determined to be a rotating disc speed of 102 rpm, a peeling duration of 87 s, and a batch load of 1.7 kg. Under these conditions, a peeling efficiency of 93%, a material loss of 8.3%, and a peeling effectiveness of 84% were achieved. Also, the performance of the machine was evaluated for different taro corms shapes and it was found that the machine performs well in the case of smooth surfaces taro corms and yields the maximum efficiency with minimum material loss. These findings demonstrate that taro corms and similar crops can be efficiently peeled using the developed machine. The peeling machine is specially designed to peel the taro corms of different shapes and is suitable for small to medium-scale industries. The peeling machine provides higher efficiency compared to other peeling machines available. Furthermore, the removed taro peel, which is often discarded as waste, can be utilized as a valuable resource for various applications, such as animal feed, bioactive compound extraction, or biofuel production. Exploring these possibilities could enhance the sustainability of taro processing by minimizing waste and increasing the economic viability of the peeling process.

Data availability

All data used for this research is included in this manuscript.

Received: 2 January 2025; Accepted: 11 March 2025
Published online: 02 April 2025

References

1. Legesse, T. & Bekele, T. Evaluation of improved taro (*Colocasia esculenta* (L.) Schott) genotypes on growth and yield performance in north-bench woreda of Bench-Sheko Zone, south-western Ethiopia. *Heliyon* https://doi.org/10.1016/j.heliyon.2021.e08630 (2021).
2. FAOSTAT. *FAO Statistical Database*; https://www.fao.org/faostat/en/#data/QCL (2024).
3. Ferdaus, Md. J., Chukwu-Munsen, E., Foguel, A. & da Silva, R. C. Taro roots: An underexploited root crop. *Nutrients* **15**(15), 3337. https://doi.org/10.3390/nu15153337 (2023).
4. Shah, Y. A. et al. Industrial applications of taro (*Colocasia esculenta*) as a novel Food Ingredient: A review. *J. Food Process. Preserv.* https://doi.org/10.1111/jfpp.16951 (2022).
5. USDA Food Composition Databases. Revised in May 2016; https://fdc.nal.usda.gov/fdc-app.html#/food-details/169308/nutrients
6. Temesgen, M. & Retta, N. Nutritional potential, health and food security benefits of taro *Colocasia esculenta* (L.): A review. *Food Sci. Qual. Manag.* **36**, 23–30 (2015).

7. Wei, Q. et al. Effects of different combined drying methods on drying uniformity and quality of dried taro slices. *Dry. Technol.* **37**(3), 322–330. https://doi.org/10.1080/07373937.2018.1445639 (2018).
8. Alcantara, R. M. The nutritional value and phytochemical components of taro [*Colocasia esculenta* (L.) schott] powder and its selected Processed Foods. *J. Nutr. Food Sci.* https://doi.org/10.4172/2155-9600.1000207 (2013).
9. Tang, C. & Sakai, W. 6 Acridity of taro and related plants. In *Taro: A Review of Colocasia esculenta and Its Potentials* (ed. Wang, J.) 148–164 (University of Hawaii Press, 1983). https://doi.org/10.1515/9780824887612-010.
10. Chai, W. & Liebman, M. Oxalate content of legumes, nuts, and grain-based flours. *J. Food Compos. Anal.* **18**(7), 723–729. https://doi.org/10.1016/j.jfca.2004.07.001 (2005).
11. Khan, S. R. & Glenton, P. A. Investigative urology: Deposition of calcium phosphate and calcium oxalate crystals in the kidneys. *J. Urol.* **153**(3), 811–817 (1995).
12. Mandel, N. S. & Mandel, G. S. Urinary tract stone disease in the United States veteran population. II. Geographical analysis of variations in composition. *J. Urol.* **142**(6), 1516–1521. https://doi.org/10.1016/s0022-5347(17)39145-0 (1989).
13. FAO. *Roots, Tubers, Plantains and Bananas in Human Nutrition* (Food and Agriculture Organization UN, 1990).
14. Yusuf, A., Sugandi, W. K. & Zaida, Z. Rancang Bangun mesin PENGUPAS talas semir (The design of Semir Taro peeling machine). *Jurnal Teknik Pertanian Lampung (J. Agric. Eng.)* **9**(1), 19. https://doi.org/10.23960/jtep-l.v9i1.19-27 (2020).
15. Balami, A. A. et al. Design and fabrication of a cocoyam (*Colocasia esculenta*) peeling machine. *Int. Food Res. J.* **23**, S65 (2016).
16. Ezeanya, N. C. Effect of speed on efficiency and throughput capacity of cocoyam peeling machine. *Int. J. Sci. Eng. Res.* **11**(6), 241–244 (2020).
17. Ojolo, S. J., Orisaleye, J. I. & Badiru, N. Design and fabrication of a yam peeling machine. *J. Eng. Res.* **21**(1), 123–132 (2016).
18. Fadeyibi, A. & Faith Ajao, O. Design and performance evaluation of a multi-tuber peeling machine. *Agri Eng.* **2**(1), 55–71. https://doi.org/10.3390/agriengineering2010004 (2020).
19. Nordiana, J., Ighodalo, O. & Ossai, H. Design and construction of a cassava tuber peeling machine. *Int. J. Trop. Agric. Food Syst.* https://doi.org/10.4314/ijotafs.v2i2.40968 (2009).
20. Putra Samitra, G., Setiawan, C. & Siman, J. Design and build a cassava peeling machine to increase productivity. *Jurnal Riset Ilmu Teknik* **1**(3), 128–138. https://doi.org/10.59976/jurit.v1i3.26 (2023).
21. Vithu, P., Dash, S. K., Rayaguru, K. & Pal, U. S. Study on optimization of mechanical peeling for sweet potato. *Agric. Eng. Today* **44**(01), 1–7. https://doi.org/10.52151/aet2020441.1512 (2020).
22. Fadeyibi, A. & Osunde, Z. D. Thermo-physical properties of Rubber Seed useful in the design of storage structure. *Int. J. Agric. Biol. Eng.* **5**(2), 1–5 (2012).
23. Azargohar, R. & Dalai, A. K. Production of activated carbon from Luscar char: Experimental and modeling studies. *Microporous Mesoporous Mater.* **85**(3), 219–225. https://doi.org/10.1016/j.micromeso.2005.06.018 (2005).
24. Myers, R. H., Montgomery, D. C. & Anderson-Cook, C. M. *Response Surface Methodology: Process and Product Optimization Using Designed Experiments* 4th edn. (Wiley, 2016).
25. Olukunle, O. J. & Akinnuli, B. O. Performance evaluation of a single action cassava peeling machine. *J. Emerg. Trends Eng. Appl. Sci.* **3**(5), 806–811 (2012).
26. Daniyan, I. A., Adeodu, A. O., Azeez, T. M., Dada, O. M. & Olafare, A. O. Optimization of peeling time and operational speed for cassava peeling using central composite design and response surface methodology. *Int. J. Eng. Sci. Res. Technol.* **5**(9), 630–639. https://doi.org/10.5281/zenodo.155086 (2016).
27. Singh, K. K. & Shukla, B. D. Abrasive peeling of potatoes. *J. Food Eng.* **26**(4), 431–442. https://doi.org/10.1016/0260-8774(94)00065-h (1995).
28. Nagar, C. K., Dash, S. K. & Rayaguru, K. Optimization of machine parameters for the peeling of taro (*Colocasia esculenta*) mother corm in a commercial abrasive peeler. *Int. J. Plant Soil Sci.* 1218–1232 (2022).
29. Enomfon J. Akpan, & I.B. Umoh. Effect of heat and tetracycline treatments on the food quality and acridity factors in cocoyam [xanthosoma sagittifolium (L) schott]. *Pakistan Journal of Nutrition*. **3**(4), 240–243. https://doi.org/10.3923/pjn.2004.240.243 (2004).
30. Ogunlowo, S., Olaleye, S. A., & Fasunla, M. S. Performance evaluation of the automated system for cleaning, peeling and washing cassava tubers. *International Journal of Advances in Agricultural and Environmental Engineering.* **3**(2), 327–332. https://doi.org/10.15242/ijaaee.u0716202 (2016).
31. Khurmi, R. S., & Gupta, J. K. A textbook of machine design. S. Chand Limited. (2008).

Acknowledgements

All the authors would like to acknowledge the ICAR-Central Institute of Post Harvest Engineering and Technology (CIPHET), Ludhiana, India for the support provided to carry out our work.

Author contributions

S. M.: Design, conceptualization, investigation, manuscript writing, and validation; A. K. D.: Conceptualization, Methodology, Manuscript Writing- Review and Editing.; A. S.: Investigation, Formal Analysis, Software, Validation, and Manuscript Editing.

Funding

This research work is funded by the ICAR-Central Institute of Post-Harvest Engineering and Technology (CIPHET), Ludhiana.

Declarations

Competing interests

The authors declare no competing interests.

Consent for publication

The authors hereby give their consent for the publication of this work/material/image, etc. in any form or medium, with due acknowledgment.

Additional information

Correspondence and requests for materials should be addressed to A.S.